Journal of Physics: Conference Series **2380** (2022) 012022 doi:10.1088/1742-6596/2380/1/012022

Using Artificial Immune Systems to Sort and Shim Insertion Devices at Diamond Light Source

Joss Whittle
Rosalind Franklin Institute, Oxfordshire
E-mail: joss.whittle@rfi.ac.uk

Mark Basham
Rosalind Franklin Institute, Oxfordshire
E-mail: mark.basham@rfi.ac.uk

Zena Patel
Diamond Light Source, Oxfordshire
E-mail: zena.patel@diamond.ac.uk

Edward Rial
Helmholtz-Zentrum, Berlin
E-mail: edward.rial@helmholtz-berlin.de

Robert Oates
Blackberry QNX
E-mail: dr.bob.oates@gmail.com

Yousef Moazzam
Diamond Light Source, Oxfordshire
E-mail: yousef.moazzam@diamond.ac.uk

Abstract. This work presents the Opt-ID software developed by the Rosalind Franklin Institute (RFI) and Diamond Light Source (DLS) in collaboration with Helmholtz-Zentrum Berlin (HZB). Opt-ID allows for efficient simulation of synchrotron Insertion Devices (ID) and the $\mathcal{B}$ fields produced by a given arrangement of candidate magnets. It provides an optimization framework built on the Artificial Immune System (AIS) algorithm for swapping and adjusting magnets within an ID to observe how these changes would affect the magnetic field of a real-world device, guiding ID builders in the steps they should take during ID tuning. Code for Opt-ID is provided open-source under the Apache-2.0 License on Github: https://github.com/rosalindfranklininstitute/Opt-ID

1. Introduction

Optimizing an Insertion Device (ID) is a delicate and time-consuming process that is necessary to reach the exacting tolerances required by synchrotron storage rings and beamline science applications. Due to minor imperfections of permanent magnets commonly used to construct undulators, careful ordering and arrangement of magnets is needed to ensure the ID can produce light with the highest achievable brilliance. Determining an optimal ordering for a set of magnets is a complex and labour-intensive process where an initial ordering of magnets is assembled, then modified through iterative refinement guided by measurements of the $\mathcal{B}$ field produced by the device. To handle the extremely large combinatorial search space, many ID groups use simulation driven optimization to search for a strong initial magnet ordering to begin assembly, often based on well established methods such as Simulated Annealing (SA) [7, 9] and Genetic Algorithms (GA) [5].

This work presents Opt-ID, a novel software framework written in Python that applies state-of-the-art optimization and simulation techniques to efficiently search for well-performing magnet configurations. Opt-ID leverages the AIS algorithm [15, 8, 11], which dynamically balances wide exploration of the search space against focused exploitation of well-performing regions, and is built on prior work on SA sort code written in Fortran 77. Along with searching for a strong initial magnet configuration in-simulation, Opt-ID incorporates real-world field measurements to guide construction through iterative phases of trajectory shimming and re-measurement, narrowing the reality-gap and reducing the number of physical alterations that need to be performed to tune an ID. Changes to the device $\mathcal{B}$ field are efficiently calculated using lookup-tables, enabling Opt-ID to iterate through a greater number of candidate magnet orderings within a fixed computation budget. Opt-ID and AIS scale robustly across distributed and heterogeneous compute resources, further increasing its efficacy at exploring the search space.

At DLS, a modern 3rd generation synchrotron, Opt-ID has been used to efficiently sort and shim IDs of various designs including PPM, hybrid CPMU, and APPLE-II undulators.

2. Tuning IDs

When optimizing IDs the goal is to maximize the brilliance of the emitted light. Brilliance (equation 1) is a function of the rate at which photons are emitted over time, the angular divergence of the photon beam, the cross-sectional area of the electron beam, and how tightly grouped the emitted wavelengths are around the target wavelength [14, 10].

$$\text{brilliance} = \frac{\text{photons}}{\text{second} \cdot \text{mrad}^2 \cdot \text{mm}^2 \cdot 0.1\%\text{BW}} \tag{1}$$

Some terms in the brilliance equation are more feasible to tune than others when optimizing an ID. Photon rate is largely controlled by the number of periods in the ID meaning to increase brilliance more periods need to be added, leading to a longer device. Minimizing the angular divergence of the photon beam increases brilliance by ensuring that more photons make it downrange to the target. As the velocity of the electron beam approaches the speed of light, the upper-bound on angular divergence is decreased due to relativistic effect which pushes the directional profile for photon emission towards a Dirac distribution. Shrinking the cross-sectional area of the electron beam focuses the aperture in the XZ-plane where photons are being emitted along the length of the device. Lastly, consistency of oscillations in $\mathcal{B}$ field along the ID controls the purity of the emitted wavelengths in the photon beam.

In practice, maximum device length, electron beam energy, and lower-bounds on angular divergence and cross-sectional area will all be constant when optimizing an ID for a given synchrotron facility. Magnet geometry, material, ideal field vectors, and device arrangement

are determined through an initial design and optimization procedure such that the ideal device has the desired properties such as photon wavelength and polarization. Magnet geometry is chosen to balance the desired effect on the device $\mathcal{B}$ field against the engineering and logistical constraints of needing to be able to clamp magnets in accurate positions and orientations within device girders.

Maximizing brilliance with these external constraints, a chosen ID design, and a set of precisely manufactured candidate magnets, therefore simplifies to considering how to best compensate for the manufacturing tolerances and deviations of each magnet during the assembly procedure.

2.1. Initial Sorting

Assembly begins by constructing a rough device from a random or hand selected configuration of magnets, or one chosen by sorting an initial magnet arrangement in simulation. The latter approach is often realized based on optimization strategies such as SA [13, 7, 9], GA [12, 5], or in the case of this work by using AIS [15, 8, 11].

After the rough device has been assembled, the $\mathcal{B}$ field is measured at regular intervals along the centre-line of the device and used to visualize the suitability of the current arrangement. At DLS and in common with many ID labs, a three-axis Hall probe mounted on a linear rail running parallel to the ID is used for magnetic field mapping and a copper flipping coil is used for field integral measurements [2]. The Hall probe and flipping coil are controlled with Igor Pro [18] using software supplied by ESRF [4, 6].

2.2. Trajectory Shimming

From an initial magnet sort the electron trajectories produced by the ID are tuned to remove undesirable drifts and deflections (figure 1) by using the measured $\mathcal{B}$ field data to select a number of modifications that are predicted to best correct the observed trajectory errors. These modifications are applied to the device and it is re-measured using the Hall probe. This process then repeats until builders are satisfied that any major trajectory drifts or deflections have been compensated for as best as possible.

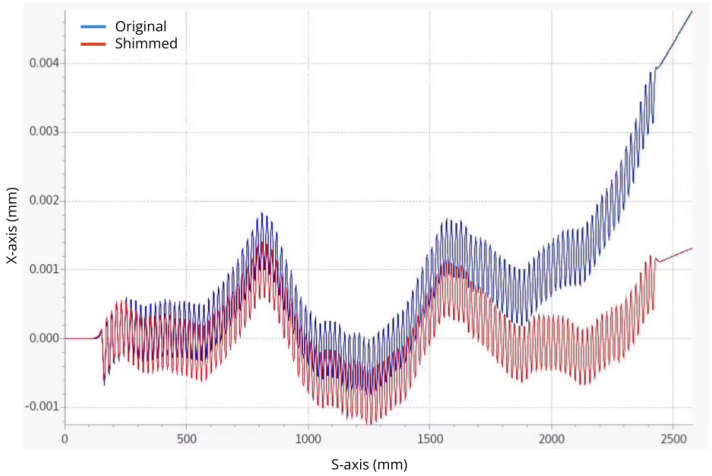

Figure 1: The effect of a trajectory shimming iteration on electron trajectories in a CPMU ID. A small number of carefully selected modifications can have a significant impact on correcting trajectory errors.

In each iteration only a small number of modifications are made (approximately 5 per iteration at DLS). This ensures both a fast turn-around on each iteration between re-measurements, and also mitigates the compounding effects of the reality-gap, where predictions about the effect a given modification will have become less accurate as increasing numbers of modifications are applied in-simulation before the field is re-measured.

3. Magnet Imperfections

To search for well-performing configurations, the effects of magnet errors on the device $\mathcal{B}$ field need to be characterized. At DLS and in Opt-ID magnets are characterized by their size and measured field vectors compared to the idealized size and field vector for a perfect magnet of that type. Magnet suppliers used by DLS usually achieve dimensional tolerance within ± 40 microns and angular magnetic field tolerance within approximately $\pm 1°$. Even at this precision significant error will accumulate along the length of an ID and its many magnet elements.

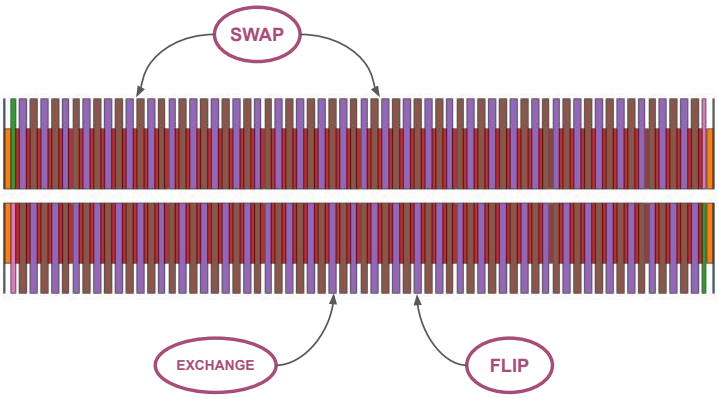

Figure 2: Different magnet operations used during sorting and trajectory shimming shown on the geometry of a 32 period hybrid CPMU ID. Compatible magnets can be swapped with one another within the device, exchanged with an unused spare magnet, or flipped in-place within a magnet slot.

To compensate for the deviances of each magnet element and control their combined effects on field error there are several ways that IDs can be modified to mitigate the accumulated error along the length of an ID:

Swap operations to the ID are performed by selecting two slots in the device for the same type of magnet and swapping their currently selected magnets with one another. If the two slots that are selected refer to different major field directions, i.e. vertical up and down slots or horizontal front and back slots then magnet elements are flipped as appropriate so that their major field axis aligns with the new slot.

Exchange operations are similar to swaps except only one slot is chosen from the device, and the second magnet that will be exchanged is chosen from a set of unused spares of the same type. Due to the potential for magnet elements to become damaged or to have unacceptably large error in their manufactured tolerances ID builders at DLS typically order $\approx 20\% - 50\%$ more magnets of each type than are required by the design to allow for exchanges to be made during tuning.

Flip operations are generally achieved by a 180° rotation around the major field axis of the magnet element. This has the effect of reversing the two minor field axes of the magnet while maintaining the major field axis, steering the direction of its errors (figure 3). Unlike swap and exchange operations that can be applied to any magnet candidate and device slots of the

same magnet type, flip operations require special care to ensure that symmetries in the magnet geometry are respected.

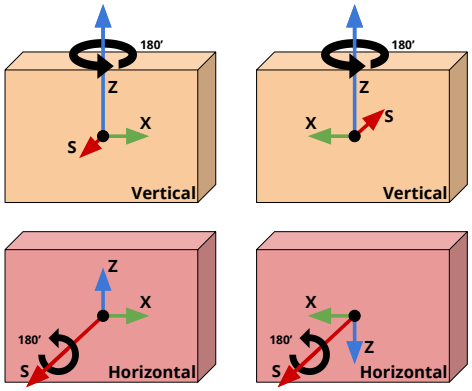

Figure 3: Applying flip operations to magnet elements over their symmetries. Top: Vertical magnets with major fields aligned to the Z-axis. Bottom: Horizontal magnets with major fields aligned to the S-axis

Figure 4 highlights the constraints imposed by magnet geometry and holder design. Both vertically and horizontally aligned PPM magnets can be flipped about their major field axes by 180° while maintaining their respective geometries (figure 4b). For APPLE-II magnets however, due to the asymmetry of the square-cut corners, applying a flip operation about the Z-axis for vertically aligned magnets would result in the square-cut corners being on the incorrect sides, preventing it from fitting in the holder (figure 4a).

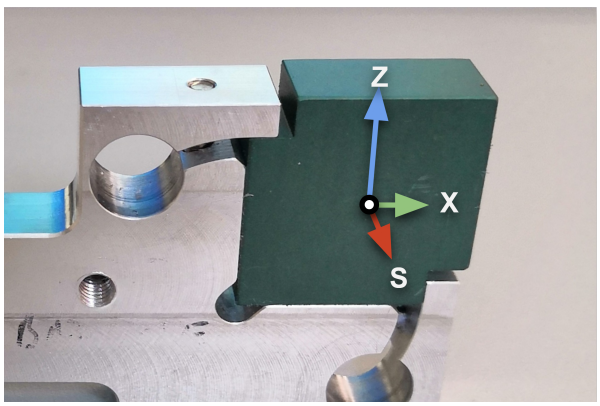

(a) APPLE-II type magnet in its holder

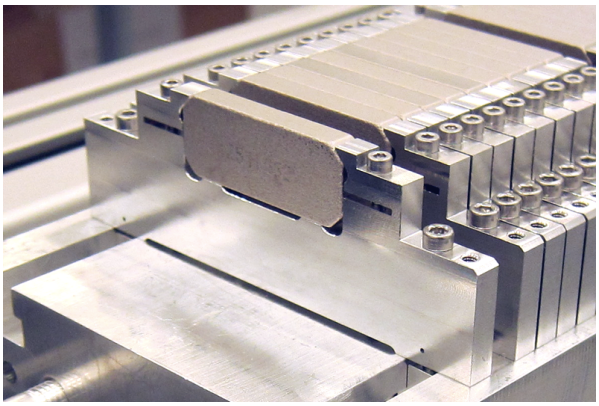

(b) PPM type magnet in its holder

Figure 4: Magnet geometry and mounting methods effect which symmetries and flip configurations are available for differently aligned magnets. Left: The square-cut corners used for clamping the magnet means it only has symmetry about the S-axis, preventing magnets with a vertical major field axis from being flipped. Right: The magnet geometry is symmetric about both the Z and S axes, allowing magnets with both horizontal and vertical major field axes to be flipped through 180°.

4. Search Space Complexity

The search space of all possible magnet orderings and flip states is prohibitively large to cover with a brute-force approach. Further, it is extremely sparse with small islands of well-performing

magnet orderings surrounded by vast gulfs of poorly performing configurations.

Table 1: Search space for a PPM type ID composed of horizontal (HH) and vertical (VV) magnets, with two accompanying kicker magnets (HE and VE) at the ends of both girders.

Magnet Type	Candidates	Slots	Complexity
HH	576	402	$\approx 10^{1025}$
VV	576	402	$\approx 10^{1025}$
HE	24	4	255024
VE	24	4	255024

Table 1 shows the search space complexity for each magnet type of a 100-period PPM device composed of four types of magnet. The complexity of the marginal search space for each magnet type can be modelled as: Choose S magnets from C candidates without replacement, where permutation of selection matters, including both flipped and un-flipped variations on each slot. Equation 2 models complexity of the full ID as the product of the marginal complexities over the set of magnet types T.

$$10^{2056} \approx \prod_{t \in T} \frac{C_t!}{(C_t - S_t)!} 2^{S_t} \tag{2}$$

Even for comparatively small areas of the of the search space such as the marginal HE and VE orderings based on only 24 candidates and 4 slots each, the joint search space of both HE and VE together already explodes to 65 billion possible configurations. For the full search space the problem quickly becomes intractable on the order of 10^{2056} configurations.

5. Artificial Immune Systems

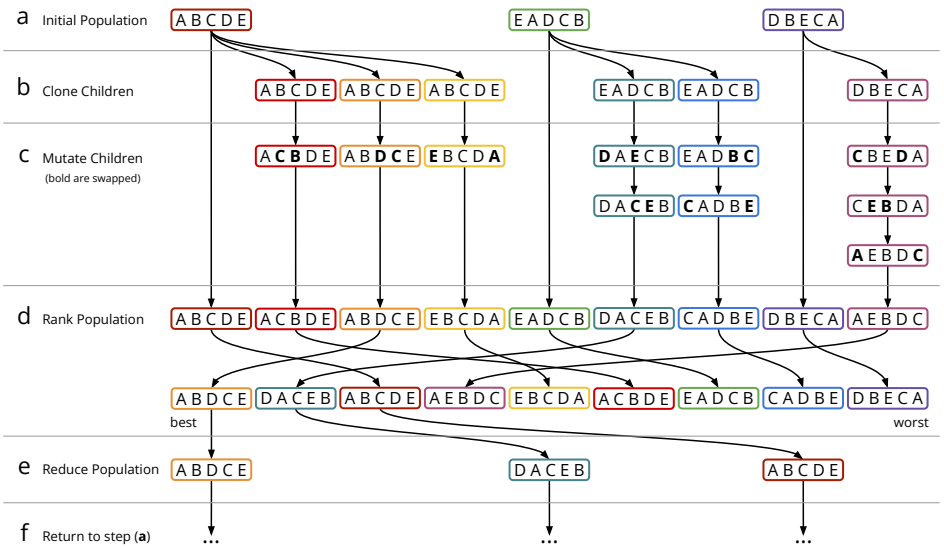

Figure 5: An iteration of AIS optimization on a population of candidate orderings. Candidates are visualized as a small permutation of 5 characters A-E without duplicates. Bold characters highlight where mutations to the orderings have been applied.

Opt-ID uses the AIS algorithm [15, 8, 11] to optimize a population of magnet orderings in search of well-performing candidates. Figure 5 shows an overview of an iteration of AIS acting on

a small population of three ranked candidate orderings (shown as permutations on the characters A-E without duplicates) **(a)**. For each candidate magnet ordering x_i in the ranked population compute $N, M = H_i(x_i)$, and **(b)** generate N clones $x'_{i,1} \dots x'_{i,N}$ and **(c)** mutate them M times each. The original population combined with the new mutated candidates are then ranked by an objective function **(d)** and the top-k are selected to form the population for the next AIS iteration **(e)**.

The heuristic $N, M = H_i(x_i)$ is chosen such that best performing candidates are cloned wider and mutated shallowly to focus more computation into exploring well-performing regions of the search space, while candidates with poorer performance are cloned narrowly and mutated deeply in the hope this will allow them to traverse sparse regions of the search space to where they may find better performing regions. Thus balancing wide exploration of the search space against targeted exploitation of regions that are believed to contain strong solutions.

5.1. Comparison to Other Optimization Methods

There are many approaches to tackling optimization on large and sparse search spaces often based on SA [13, 7, 9] or GA [12, 5] methods, each with their own caveats. GA require careful design of mutations to ensure combinatorial constraints of the search space are respected (such as using each magnet in only one slot at a time), and SA based methods can struggle to sufficiently explore well-performing regions of the search space once they are identified before moving on to potentially less advantageous regions.

SA can be interpreted as taking a (or many independent) random walk through the search space. At each iteration a candidate mutation is proposed, and is accepted or rejected randomly. Often the probability of accepting a candidate is adjusted globally over the length of the optimization process according to a "cooling" schedule such that early in the optimization mutations are largely accepted, giving wide coverage of the search space, and towards the end of the optimization mutations are largely rejected providing stable convergence to at least a local optimum.

Design of the cooling schedule has a significant impact on the convergence of the SA algorithm and the quality of its proposed solutions. The schedule must be tuned to each optimization problem which is often an expensive and non-trivial meta-optimization. Further, as the schedule cools it becomes decreasingly likely a suggested mutation will be accepted, leading to redundant and wasted computation in the later parts of the optimization. In AIS the design of the heuristic for balancing clones vs mutations for each candidate has a similar impact on the quality of convergence but tends to be significantly more robust to poor tuning given the amount of information that is shared across the population at each iteration.

Figure 6 shows an equal computation comparison between AIS and SA when performing the initial sort optimization of a 113 period CPMU device. Because the computation is dominated by evaluating the objective function this is also an equal time comparison. Both algorithms used a population size of 24 and performed an equivalent number of mutation operations over the run. AIS used generic un-tuned hyper-parameters for controlling the exploration that have shown to be robust in many conditions, while for SA time was spent tuning hyper-parameters and the best performing run is reported.

AIS is able to rapidly and stably converge to a strong solution and exhibits good performance across the population due to the ranking and filtering phase at each iteration. SA, which does not communicate information across the population, shows higher variance and at several points during the run spends significant time in regions that perform worse than previously identified solutions. After 1000 iterations both algorithms are still steadily improving the quality of their solutions, however it is clear that AIS has converged faster and more stably towards a stronger set of candidates.

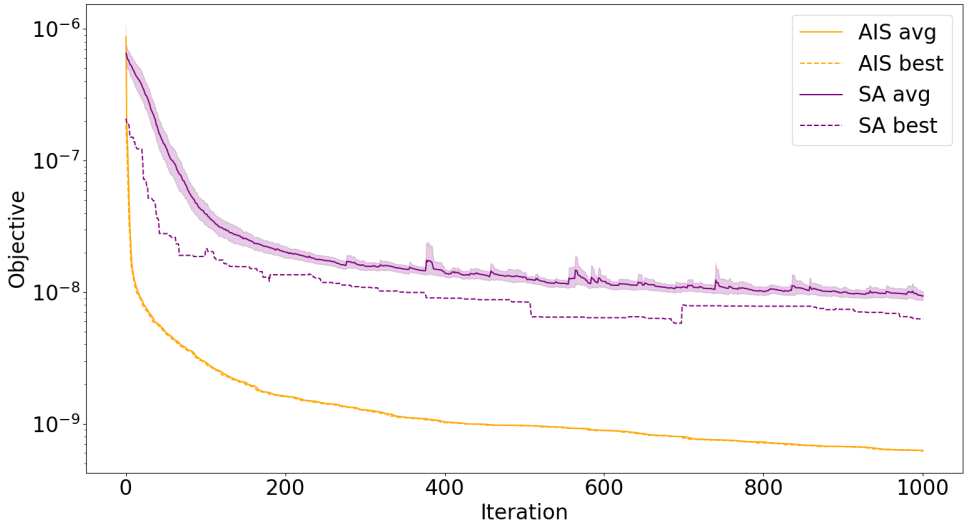

Figure 6: Equal computation/time comparison of AIS vs SA when performing the initial sort optimization of a 113 period CPMU device. Both algorithms used a population size of 24 and performed an equivalent number of mutations over the run. Dashed lines show the fitness of the best candidate in the population at each iteration while the solid lines and error bars show the mean and standard deviation across the population.

5.2. Distributed Optimization

Both SA and AIS can benefit greatly from executing in distributed compute environments allowing for more magnet orderings to be simulated and compared, increasing the likelihood of discovering well-performing regions of the search space. While scaling SA is trivial due to its embarrassingly parallel nature, AIS requires periodically communicating the local populations of each node.

Figure 7 shows a high level overview of distributed AIS, where each parallel node of the computation starts by making one or more optimization iterations to its local population (figure 5) before all-to-all communicating to one another so that each node has the global population. Nodes then independently form a consensus by ranking their copy of global population, before finally each node takes a non-overlapping subset of the ranked population such that each gets a fair balance of the best performing candidates.

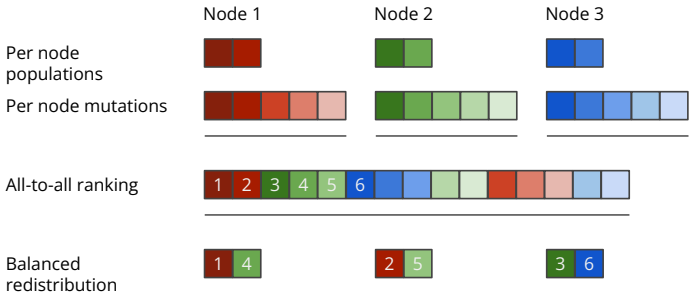

Figure 7: Distributed AIS communicating local populations of candidates between nodes and redistributing the top-k candidates fairly to keep all nodes operating in well-performing but diverse regions of the search space.

Distributed AIS has the effect of keeping all nodes working on areas of the search space that are likely to contain or be adjacent to well-performing magnet orderings throughout the

optimization process. This is preferable to distributed SA using many independent random walks over the search space, where it is likely that nodes will spend a lot of their time with local populations containing many poorly performing candidates.

6. Efficiently Computing B Fields

Computing high-fidelity $\mathcal{B}$ fields is vital to closing the reality-gap between simulation and real-world measurement of IDs. However, for large IDs containing many hundreds or thousands of magnet elements re-simulating the full field after each mutation would be prohibitively expensive, limiting the number of candidate orderings that can be explored.

Without considering the non-linear field contributions of the ID (such as iron poles in hybrid CPMU devices), Opt-ID assumes unit-permeability of the magnets, allowing the full ID $\mathcal{B}$ field to be approximated by the element-wise sum of independent fields for each magnet sampled over the same lattice of world-space coordinates (figure 8).

The lattice of coordinates used by Opt-ID is user defined, but in-general chosen to be a tightly focused, 3×3 Cartesian grid centred and extruded along the path of the electron beam with a small step size of 0.1mm in the X- and Z-axes. The step size along the S-axis is the most vital parameter for achieving high-fidelity optimization of the device field, chosen such that a constant number of samples is taken for each magnet element along the device with good resolution. Commonly a step size of $1/20^{th}$ of the period length is used at DLS.

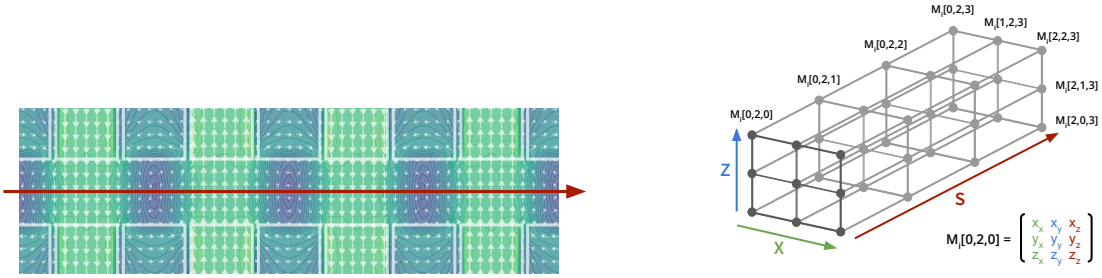

(a) $\mathcal{B}$ field (b) Lookup-table lattice of matrices

Figure 8: Sampling lattices used to evaluate $\mathcal{B}$ fields efficiently. Left: A cross section view of the ZS-plane showing the $\mathcal{B}$ field of a simulated PPM device with a 1mm gap. Along the centre-line the red arrow shows location of the sampling lattice, while the outlines of the inner edges of the magnets are shown in white. Right: An orthogonal sampling lattice of affine matrices.

Given the current device and its approximated $\mathcal{B}$ field, applying a mutation simplifies to subtracting the field contribution of the magnet currently in a device slot and adding the field of a new magnet in a given orientation. This in-place update of the field can introduce some variance over many iterative modifications due to floating point error, but this can be mitigated by periodically re-summing over the full ID to place an upper-bound on the accumulated error.

Opt-ID further accelerates simulating the per-magnet $\mathcal{B}$ fields using lookup-tables for each magnet slot within the device. Consider $\mathcal{B}_{c,i}$ as the field of a given candidate magnet c placed in the i^{th} slot of the device sampled over a regular lattice of world-space coordinates, as a tensor with shape $(X, Z, S, 3)$ that is dependent on the major field vector of the candidate magnet $\mathcal{F}_c$ which contains some error. Rather than directly simulating $\mathcal{B}_{c,i}$ on-the-fly, Opt-ID pre-computes a lookup-table $\mathcal{M}_i$ for the i^{th} slot as a matrix-valued lattice with shape $(X, Z, S, 3, 3)$ where the elements are affine scale + rotation matrices that transform the candidate field vectors $\mathcal{F}_c$ into the $\mathcal{B}$ field vector for each location on the sampling lattice through broadcast matrix multiplication $\mathcal{B}_{c,i} = \mathcal{F}_c \bigotimes \mathcal{M}_i$. The matrix elements of $\mathcal{M}_i$ are computed by stacking orthogonal-basis fields

$\mathcal{B}_{X,i}$, $\mathcal{B}_{Z,i}$, and $\mathcal{B}_{S,i}$ along their trailing axis (figure 8b, lower right), where the basis fields are simulated assuming an ideal magnet is placed in slot i with major field vector aligned to the basis with unit magnitude.

Opt-ID currently uses a stretched-wire approximation of rectangular magnet elements, with limited support for some complex geometry such as the square-cut corners commonly featured on APPLE-II type magnets. An open area of development within Opt-ID is allowing for multiple back-end magnetostatic solvers such as Radia [3] and the development of novel GPU based solvers.

7. Objective Functions

In order to perform optimization over a population of candidate magnet orderings it is necessary to evaluate each ordering such that they can be compared and ranked. Designing objective functions that are robust and provide a meaningful landscape on the search space to optimize over is vital to achieving good stability and strong solutions [1].

Early in the development of Opt-ID while drawing from an existing SA based implementation, a multi-objective loss function was used which balanced multiple statistics about the candidate orderings $\mathcal{B}$ field, the projected electron trajectories through the field, and the estimated phase-error [16, 17] of those trajectories. Trajectories can be evaluated efficiently in Opt-ID by integrating along the S-axis of the a $\mathcal{B}$ field lattice using the trapezoidal rule. This can then extend to approximating the phase-error by performing a straight line fit over the trajectories and summarizing the peak locations of each oscillation.

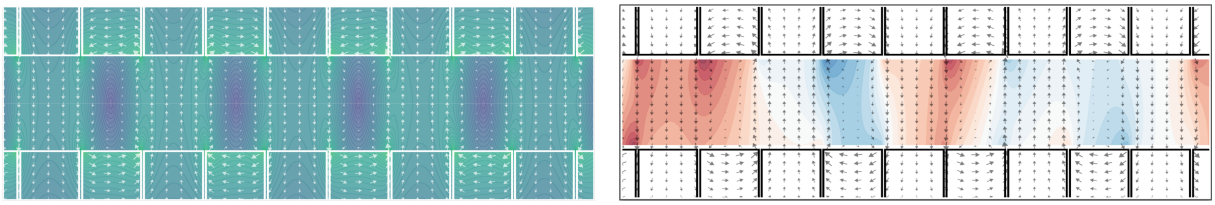

(a) $\mathcal{B}$ field (b) Error

Figure 9: Cross sectional view of the ZS-plane for a simulated hybrid CPMU device with a 1mm gap. Left: The $\mathcal{B}$ field. Right: $\mathcal{B}$ field error shown in a blue $\longrightarrow$ red colour denoting reduced $\longrightarrow$ increased field strength compared to the ideal field produced by perfect magnets. Along the top and bottom the outlines of the inner edges of the magnets and iron poles are shown in white (left) and black (right)

Achieving the delicate balance between multiple objectives required manual tuning which varied when simulating different designs and lengths of ID, often leading to poor optimization performance and a confusing user experience. Through experimentation it was found that a much simpler approach was to directly consider the divergence of the $\mathcal{B}$ field produced by the candidate magnet orderings compared to the field that would be produced by an ideal device containing magnets all with uniform field strengths and perfect alignment (figure 9). In practice, Opt-ID uses the RMSE of the candidate $\mathcal{B}$ field, while continued development of robust objective functions that incorporate domain knowledge is an open area of research (section 10).

8. Tuning IDs with Opt-ID

Opt-ID has been designed to fit around and accelerate the build methodology used at DLS. At a high-level, use of Opt-ID falls into two main phases (figure 10). First, an initial setup phase

is performed, ingesting the specification and design of the ID along with measured field vectors characterizing the manufacturing errors of each candidate magnet. From these inputs, lookup-tables are computed for each slot in the device along with the construction of data-structures for representing the candidates that remain constant during the optimization process.

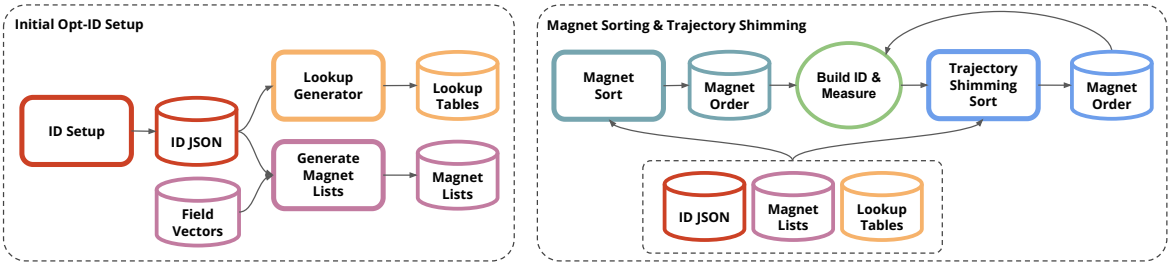

Figure 10: Tuning an ID with Opt-ID falls into two main phases. Left: An initial setup phase, where data structures are created and lookup-tables for the magnet slots computed. Right: Followed by an iterative sorting, shimming, and re-measurement phase.

In the second phase, Opt-ID is used to optimize the magnet ordering. This starts with an initial sort operation performed entirely in-simulation to discover a good initial ordering for the ID build team to assemble. From the rough assembled device, the real-world $\mathcal{B}$ field is measured and this data is used to more accurately predict how subsequent magnet modifications will alter the full field of the device.

Real-world measured field data is incorporated into the simulation by replacing the full simulated $\mathcal{B}$ field (section 6) with the measured field. The per-magnet simulated field contributions (computed from the lookup-tables) are then subtracted and added to the real-world field data. Over a small number of modifications the accuracy of the predicted full device fields is greater than that of the fields calculated fully in-simulation, becoming less reliable as increasing numbers of modifications are applied and the reality-gap widens.

9. IDs Built with Opt-ID

Opt-ID has been used at DLS since the it's inception in 2012, supporting the construction and tuning of multiple ID designs. Table 2 highlights the different types of ID that have been built using Opt-ID along with the approximate time it took to sort and shim each device.

J13 was the first device where the initial sort leveraged Opt-ID. At the time the code was almost a direct port of a prior SA based sort code written in Fortran 77, although during this period of development the lookup-table strategy for efficiently simulating device $\mathcal{B}$ fields was implemented. I21 was the first device to use Opt-ID for trajectory shimming, incorporating real world measurements of the device $\mathcal{B}$ field into the simulation to narrow the reality-gap. This was important due to the number of magnet slots on I21 leading to an extremely large search space.

Opt-ID has been developed as a "living" piece of software, tightly coupled to the needs of the DLS ID build team, and initially highly focused on solving the immediate problems faced when tuning the IDs being built at that time. Over the construction of multiple IDs of varied design, the specification for what was needed from Opt-ID and the underlying design choices for how IDs should be represented in code, and efficiently reasoned about have undergone significant refinement. Current and future work on Opt-ID aims to continue formalizing these requirements while making them increasingly agnostic to the specific build methodology used at DLS, making Opt-ID more suitable for wider adoption.

Table 2: IDs built with Opt-ID at DLS. Sort times shown as * indicate that sorting was done over a longer period, either before Opt-ID was created or while it was being actively developed to improve its capabilities.

Commissioned	ID	Type	Period	Magnets	Sort Time	Shim Time	Shim Iterations	Opt-ID Usage
1/2022	CPMU-3 / I24	Hybrid CPMU	17.6 mm	460	2 days	7 days	12	Sort & Shim
4/2021	CPMU-2 / I03	Hybrid CPMU	17.6 mm	460	2 days	15 days	34	Sort & Shim
3/2020	CPMU-1 / I24	Hybrid CPMU	17.6 mm	460	2 days	40 days	79	Sort & Shim
4/2017	J02	PPM	21 mm	770	4 days	20 days	23	Sort & Shim
9/2014	I21	APPLE-II	56 mm	1452	*	5 days	8	Sort & Shim
11/2013	J13	PPM	25 mm	434	*	16 days	9	Sort
3/2012	I09	PPM	27 mm	298	*	23 days	114	
11/2008	I14	PPM	23 mm	340	*	21 days	24	
2007	I11	PPM	22 mm	362	*	20 days	90	

10. Conclusions

In this paper we have presented Opt-ID, a novel software framework that applies state-of-the-art optimization and simulation techniques to efficiently search for well-performing ID magnet configurations. Opt-ID has been used to successfully sort and trajectory shim multiple IDs of varied design and lengths at DLS and features state-of-the-art combinatorial optimization methods using the AIS algorithm, along with an efficient method for simulating changes to ID $\mathcal{B}$ fields using pre-computed lookup-tables. There are several areas of focus for our continued development of the Opt-ID software, namely:

Adding support for complex magnet geometries to improve the accuracy of simulated $\mathcal{B}$ fields, narrowing the reality-gap between simulation and real-world field measurements. Supporting the optimization of additional steps of the tuning process such as height shimming iron poles in hybrid CPMU type IDs. Supporting arbitrary compute environments and leveraging GPUs and heterogeneous compute resources. Supporting multiple back-end frameworks for simulating $\mathcal{B}$ fields such as Radia [3]. And moving the optimization algorithms into a generic combinatorial optimization framework that Opt-ID and other projects can build on-top of.

Opt-ID will continue to become a more generalized framework for simulating and tuning IDs agnostic of the varying build methodologies used by teams at synchrotron and facilities around the world allowing it to be more easily adopted into existing workflows.

Acknowledgments

Opt-ID is a collaboration between the Rosalind Franklin Institute, Diamond Light Source, and Helmholtz-Zentrum Berlin and is generously supported by grants from the Ada Lovelace Centre and Diamond Light Source. Code for Opt-ID is provided open-source under the Apache-2.0 License on Github: `https://github.com/rosalindfranklininstitute/Opt-ID`

References

[1] BL Bobbs et al. “In search of a meaningful field-error specification for wigglers”. In: *Nuclear Instruments and Methods in Physics Research Section A: Accelerators, Spectrometers, Detectors and Associated Equipment* 296.1-3 (1990), pp. 574–578.

[2] J Chavanne et al. “Status of the European synchrotron radiation facility insertion devices”. In: *Review of Scientific Instruments* 63.1 (1992), pp. 317–320.

[3] O Chubar. *Radia*. `https://github.com/ochubar/Radia`. 2018.

[4] O Chubar and P Elleaume. "Accurate and efficient computation of synchrotron radiation in the near field region". In: *Proceedings of the European Particle Accelerator Conference*. 1998, pp. 1177–1179.

[5] O Chubar et al. "Application of genetic algorithms to sorting, swapping and shimming of the SOLEIL undulator magnets". In: *AIP Conference Proceedings*. Vol. 879. 1. American Institute of Physics. 2007, pp. 359–362.

[6] O Chubar et al. "Physical optics computer code optimized for synchrotron radiation". In: *Optical Design and Analysis Software II*. Vol. 4769. International Society for Optics and Photonics. 2002, pp. 145–151.

[7] AD Cox and BP Youngman. "Systematic selection of undulator magnets using the techniques of simulated annealing". In: *Insertion Devices for Synchrotron Sources*. Vol. 582. International Society for Optics and Photonics. 1986, pp. 91–97.

[8] V Cutello et al. "Clonal selection algorithms: a comparative case study using effective mutation potentials". In: *International Conference on Artificial Immune Systems*. Springer. 2005, pp. 13–28.

[9] Bruno Diviacco. "Performance optimization of pure permanent magnet undulators". In: *Proceedings of International Conference on Particle Accelerators*. IEEE. 1993, pp. 1590–1592.

[10] JA Holloway et al. "Brilliant X-rays using a two-stage plasma insertion device". In: *Scientific reports* 7.1 (2017), pp. 1–9.

[11] T Jansen, P Oliveto, and C Zarges. "On the analysis of the immune-inspired B-cell algorithm for the vertex cover problem". In: *International Conference on Artificial Immune Systems*. Springer. 2011, pp. 117–131.

[12] T Jansen and I Wegener. "The analysis of evolutionary algorithms - A proof that crossover really can help". In: *Algorithmica* 34.1 (2002), pp. 47–66.

[13] S Kirkpatrick, CD Gelatt, and MP Vecchi. "Optimization by simulated annealing". In: vol. 220. American Association for the Advancement of Science, 1983, pp. 671–680.

[14] Q Shen. *X-ray flux, brilliance and coherence of the proposed Cornell energy-recovery synchrotron source*. 2001.

[15] J Timmis, C Edmonds, and J Kelsey. "Assessing the performance of two immune inspired algorithms and a hybrid genetic algorithm for function optimisation". In: *Congress on Evolutionary Computation*. Vol. 1. IEEE. 2004, pp. 1044–1051.

[16] RP Walker. "Interference effects in undulator and wiggler radiation sources". In: *Nuclear Instruments and Methods in Physics Research Section A: Accelerators, Spectrometers, Detectors and Associated Equipment* 335.1-2 (1993), pp. 328–337.

[17] RP Walker. "Phase errors and their effect on undulator radiation properties". In: *Physical Review Special Topics-Accelerators and Beams* 16.1 (2013).

[18] WaveMetrics. *Igor Pro*. 2018.